Microwave radiation by a relativistic electron beam propagation through low-pressure air

S. Jordan, A. Ben-Amar Baranga, G. Benford, D. Tzach,[a] and K. Kato[b]
Department of Physics, University of California, Irvine, California 92717

(Received 12 June 1984; accepted 13 August 1984)

Intense relativistic electron beams fired into air at varying pressures display a wide range of microwave signatures. These experiments held beam current, energy, and pulse length constant while varying gas pressure. Our observing window is 10 to 40 GHz. At low pressures (< 10 mTorr) exponential spectra result, consistent with beam reflexing or virtual cathode oscillations. Above 20 mTorr the spectrum flattens and suggests collective emission at the beam-generated plasma frequencies. Power falls linearly with pressure above 20 mTorr, until electron-Neutral collisions damp the emission at a few Torr. However, weak 10 GHz emission appears at full atmospheric pressure.

I. INTRODUCTION

Though transport of intense electron beams is much studied,[1-9] electromagnetic radiation is seldom measured. We made absolute power measurements at a wide range of air pressures, and here present tentative explanations of the observations, using ideas developed to explain emission from electron beams in plasma.[10-15]

II. EXPERIMENTS

The experimental apparatus was detailed elsewhere[1] and it will be described here only briefly. An approximately 50 nsec relativistic electron beam (REB) of 0.8 MV and 120 kA, produced by a relativistic electron beam source,[2] is fired into an evacuated stainless steel drift tube (20 cm diameter, 150 cm length). The matched 7Ω vacuum diode (connected to the Marx generator through a coaxial oil pulse-forming line) has a graphite annular cathode ($d = 6.5$ cm, $\Delta d = 1$ cm). For low neutral gas (air) pressures, $p < 20$ mTorr, we used a "foil-less" configuration with a 1 mm flat graphite plate anode, that had a 7.2 cm diameter hole in the center to match the cathode. For higher pressures we used a 25 μm titanium foil for the anode, this foil separated the vacuum diode from the gas-filled drift tube. The diagnostic probes and microwave horns entered the drift tube through several ports.

We performed some shots at atmospheric pressure by firing the beam through an adjustable pressure prechamber and then into air. This prechamber was a stainless steel tube closed at the two ends by 25 μm titanium foil; one of these foils served at the same time as the anode.

The microwave spectrum was analyzed by an array of bandpass filters for low frequencies, $f \leqslant 12$ GHz, and by two grating spectrometers for $12 < f \leqslant 40$ GHz. The signals for the detection diodes were recorded from fast oscilloscopes on Polaroid film. The resulting photographs were digitized and computer analyzed. The absolute power at each frequency was calculated and normalized to the area of the drift tube by using the calibrations for the detectors, variable attenuators, horns, transmitting lines, and spectrometers.

Figure 1 shows the calibrated and normalized microwave peak power versus neutral gas pressure for different frequencies. At very low pressures, $p < 1$ mTorr, there is a very slow decay in power with the pressure, especially at low frequencies such as 7 and 9 GHz. At pressures above 20 mTorr the decay is faster and we can see a linear behavior on the log–log graph, which means a power decay as (pressure)$^{-1}$ for the low frequencies and a (pressure)$^{-2}$ decay at the higher ones. The radiation was under our measurable power threshold for pressures above a few Torrs. In between these two pressure domains there is a transition monotonic at low frequencies that peaks around 10 mTorr as the frequency goes higher.

Qualitatively, we can explain this behavior by reflexing

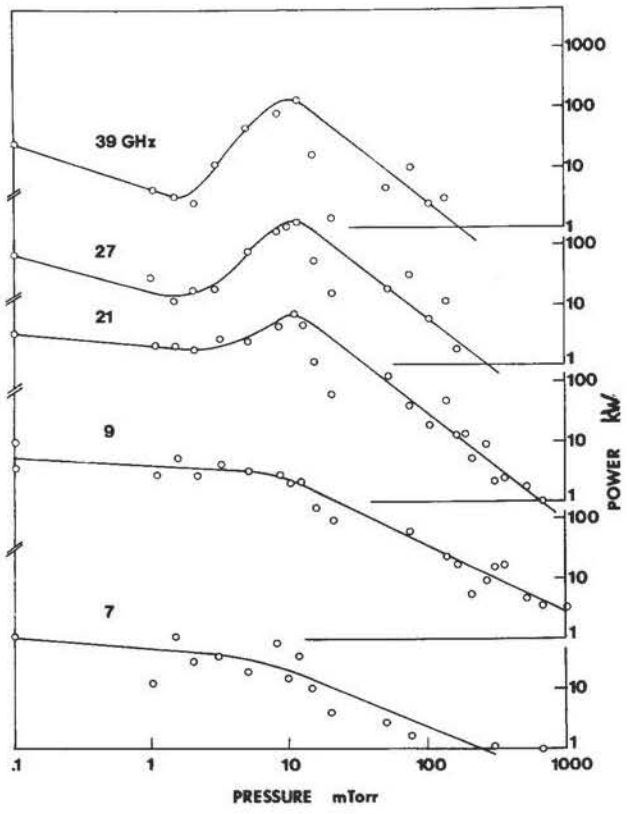

FIG. 1. Emitted power versus pressure for 7, 9, and 21 and 39 GHz.

[a] Present address: Ministry of Defense, Box 2250, Haifa, Israel.
[b] Present address: General Dynamics MZ 401-10, Box 2507, Pomona, California 91769.

 0031-9171/85/010366-06$01.90

radiation at very low pressure and by plasma formation (together with better beam propagation) at higher pressures. Apparently, the 1–20 mTorr marks the transition between these two mechanisms. At high frequency the second mechanism contribution is more significant, as there is less radiation form reflexing at these frequencies (see Fig. 4). This explains the peak in power at ~ 10 mTorr pressure at these frequencies. Above 20 mTorr the density of plasma produced by the beam in the neutral gas is high; ω_p lies in the microwave domain, but it grows quickly during the beam pulse. This is reflected in short microwave pulses above approximately 15 GHz, as ω_p changes, with longer pulses below 15 GHz. The spectrum is broader above 20 mTorr, suggesting a different emission mechanism.

Figure 2 shows the full width at half maximum (FWHM) time of the microwave radiation pulse at different frequencies versus neutral gas pressure. At very low pressure, $p < 1$ mTorr, the microwave pulse matches the REB pulse duration, i.e., radiation during all the 50 nsec electron pulse duration. This agrees with the reflexing mechanism of microwave production. Above 1 mTorr the microwave pulse duration decays fast, with the duration being around 20 nsec at 10 mTorr. This decay is caused by the space charge formation. Above 10 mTorr the decay continues, but at a much slower rate caused by the changes in the plasma density. Note that the turning point of about 10 mTorr corresponds to the maximum in the microwave power, and this was in the middle of the transition domain described in Fig 1.

At the very low frequency of 7 GHz there is not a fast decay in the pulse duration at low pressure. The signal duration of 20 nsec remains constant until approximately 75 mTorr, then decays slowly. This behavior suggests that the 7 GHz radiation is produced only by beam reflexing, and this is unaffected by $p < 75$ mTorr.

The dependence of the emitted energy on gas pressure is shown in Fig. 3 for three different frequencies. It shows a smooth decay with pressure for low frequencies and a peak at 10 mTorr for 21 GHz, similar to the power dependence of Fig. 1.

Figure 4 shows the microwave spectrum for two pressures: 1 and 12 mTorr. In both there is an exponential decay with the frequency, but this decay is much slower at the higher pressure representing a very broadband radiation.

The spectrum at 0.1 Torr (Fig. 5) is typical of the broader, lower power radiation seen above 20 mTorr pressure. It resembles the emission found in earlier experiments with the same apparatus that used hydrogen plasma as the target.[11] We surmise that emission at ω_p or a few harmonics of ω_p is responsible.

We made some full atmospheric pressure shots, firing the beam through a prechamber into the room. We photographed the beam with an open shutter camera and found that the best propagation (straight and stable beam for more than 1 m) occurred at approximately 1 Torr air pressure in the prechamber. The microwave radiation from such a beam may be very low and was detected only in X-band (8–12

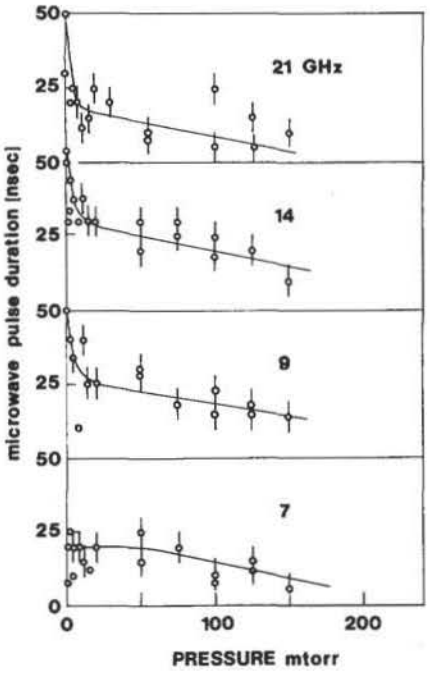

FIG. 2. Pulse duration versus neutral gas pressure for 7, 9, 14, and 21 GHz bands.

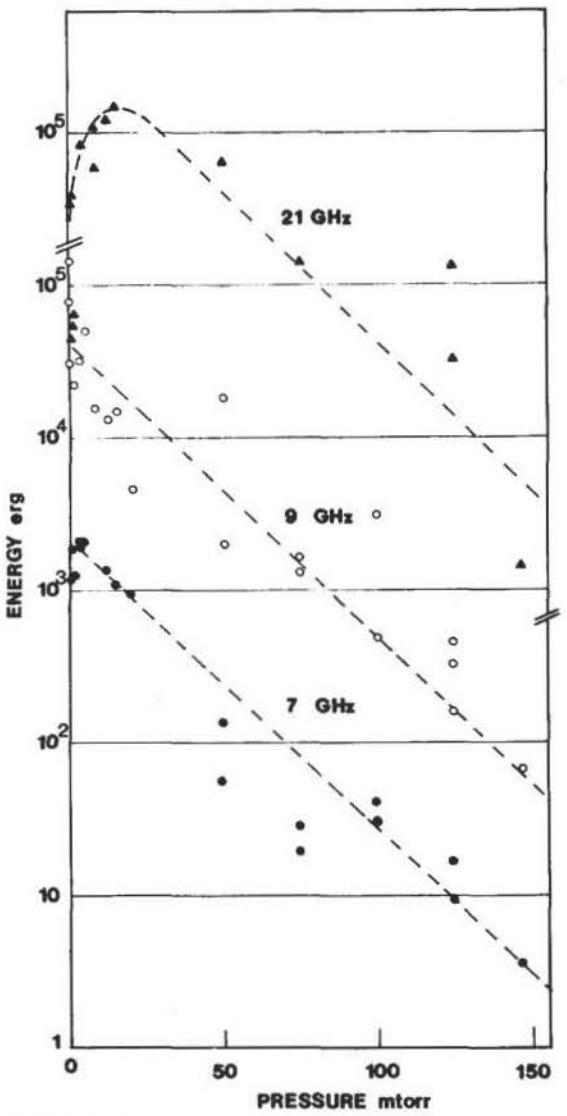

FIG. 3. Emitted energy versus neutral gas pressure for 7, 9, and 21 GHz bands.

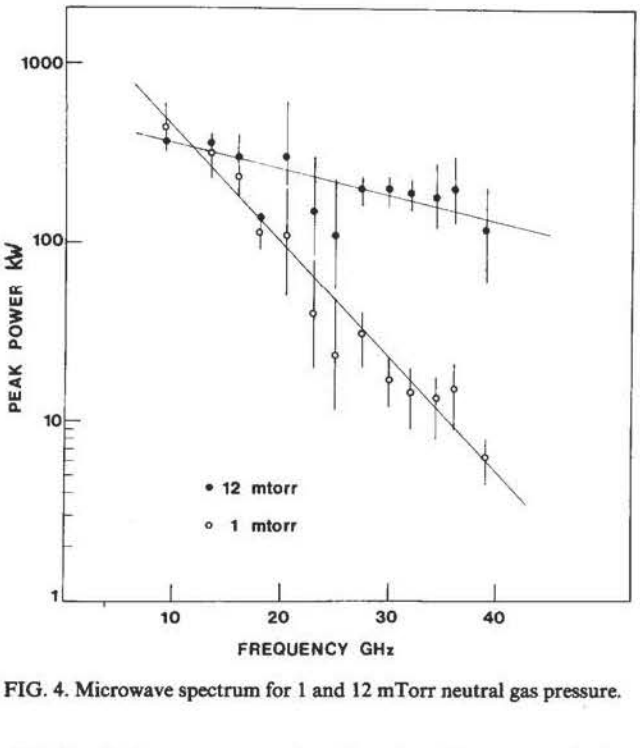

FIG. 4. Microwave spectrum for 1 and 12 mTorr neutral gas pressure.

GHz) in the beam propagation direction. To protect the horn we used a metal mirror at 45° to the beam direction to reflect the microwave radiation into the horn. We do not yet have a calibration for this measurement because of the severe electrostatic noise problems following introduction of approximately 1 coulomb of charge into the laboratory by the beam.

III. PLASMA PRODUCTION

To assess quantitatively the microwave radiation mechanisms, we calculate the gas breakdown characterisitcs in detail.

Primary electron impact ionization: The rate of change in the background ion density, $\partial n_i(t)/\partial t$, for this process is for N_2 and 1 MeV electrons:

$$\left.\frac{\partial n_i(t)}{\partial t}\right|_{\text{primary}} = \frac{n_b(t)}{\tau_e}, \tag{1}$$

where $\tau_e \sim 0.4\,[P(\text{Torr})]^{-1}$ nsec.

Secondary electron avalanche: We include ionizing collisions between neutrals and the secondary electrons, which are accelerated by the beam's unneutralized space-charge field E_r and E_z. We also subtract the loss of electrons from the region of interest:

$$\left.\frac{\partial n_e(t)}{\partial t}\right|_{\text{secondary}} = \frac{n_e(t)}{t_i} - \frac{n_e(t)}{t_s} = \frac{(t_s - t_i)n_e(t)}{t_s t_i}, \tag{2}$$

and

$$\left.\frac{\partial n_i(t)}{\partial t}\right|_{\text{secondary}} = \frac{n_e(t)}{t_i}, \tag{3}$$

where $n_e(t)$ is the number density of secondary electrons, t_s is the effective escape time of the secondary electrons from the vicinity of the beam column, and t_i is the effective secondary electron avalanche time. It is obvious that if t_s is low enough, avalanching will not be an effective ionization process, as the secondaries escape rapidly. Qualitatively, this will occur until space-charge neutralization is practically complete. Hence, E_z, the inductive axial electric field before the end of the current rise time at $t = t_r$, is the significant driving field for secondary avalanche after space-charge neutralization is achieved at $t = t_n$, when $f_e(\tau_n) = 1$. By Putnam,[9]

$$\tau_n\ (\text{nsec}) = 0.7/\beta P\ (\text{Torr}). \tag{4}$$

Space-charge neutralization is complete within our beam's rise time, approximately equal to 15 nsec for pressures over 50 mTorr. Above this pressure, secondary electron avalanche would be important between τ_n and t_r. If $\tau_n < t_r$, then a significant axial electric field of about 2×10^4 V/cm will accelerate the secondaries to ionizing velocities.[1]

Putnam calculated that secondary avalanche will continue from τ_n until gas "breakdown" occurs at $t = t_b$, after which time plasma conductivity remains essentially constant.

Ion avalanche[1,6]: Energetic ions, produced by the beam and accelerated by the unneutralized space charge and E_z, will congregate toward the center of the beam column, contributing an ionization rate

$$\left.\frac{\partial n_i(t)}{\partial t}\right|_{\text{ions}} = \frac{n_i(t)}{t_{ia}}, \tag{5}$$

where t_{ia} is the effective ion avalanche time. Charge exchange processes (which do not increase overall ionization) will proceed above some threshold ion energy. For air (which has an ionization potential comparable to hydrogen), we may reason parallel to Olson[10] and approximate this threshold ion energy as that for which the ion velocities exceed twice the velocity of a free electron in the gas. The electrons liberated in collisions betwen such ions and neturals would thus remain barely free from capture by other ions. A comfortable threshold energy for N_2 (and H_2) is then about 1.4 MeV. If the mean-free-path of the ions in the surrounding neutrals is greater than the path length required to accelerate the ions to at least this energy in the prevailing fields, ion avalanche may proceed and the ion density will increase. After charge neutralization occurs, the liberated electrons contribute to the ionization rate by cascade.

We may thus place an upper limit on pressure beyond which ion avalanche is overwhelmed by simple charge exchange. The ions are accelerated mostly by the space-charge field of the unneutralized beam, which can exceed 10^6 V/cm. Too, it is worth noting that the massive ions lose only a small fraction of their kinetic energy in each ionizing collision.

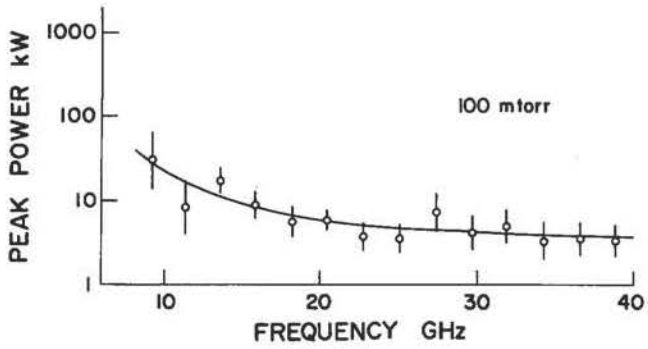

FIG. 5. Spectrum for 0.1 Torr pressure.

Hence ion ionization could continue after both neturalization and the rise time have passed.

We must depart somewhat from Olson's model of accelerated protons in a field of H_2 neutrals for our case of N_2^+ ions in (mostly) neutral nitrogen. The collision cross section differs by a factor of at least 26, and the mass ratio of the colliding particles is 28. The collision time t_{ia} depends directly on $m^{1/2}$ and inversely on the collision cross section. Hence our modification to the Olson model amounts to a factor of 0.2 and

$$t_{ia} \sim 0.07/P \text{ (Torr) nsec}$$

for pressure at which ion avalanche can proceed. These pressures, also in references to Olson's model, are those for which $28\,E\,(\text{V/cm})/P\,(\text{Torr}) < 10^6$ V/cm Torr, to a fair approximation.

For pressures below about 36 mTorr, then, ion ionization can occur before τ_n and at a decaying rate thereafter as the ion energy gradually dissipates.

Plasma density[1]: We have taken the simple collisional models advanced above and calculated, semiqualitatively, the plasma density and conductivity resulting from them as functions of time and pressure. We use numerical integration and several convenient simplifications.

(1) We presume only singly-charged ions are produced.

(2) The beam current rises linearly and falls instantaneously:

$$I(t)\begin{cases} I_p(t/t_r) & t<t_r, \\ I_p & t_r<t<t_{\text{beam}}, \\ 0 & t>t_{\text{beam}}. \end{cases}$$

(3) The secondary electrons escape instantaneously before charge neturalization at $t=\tau_n$, and thereafter remain in the vicinity of the beam column. Electron avalanche may proceed from τ_n to the lesser of t_r and t_b.

(4) Ion avalanche only proceeds at pressure below about 36 mTorr and continues at a decaying rate after τ_n.

(5) We take $t_r = 15$ nsec. Here E_z is the accelerating field for electron avalanche, and we ignore the inductive E_z field for ion avalanche.

(6) The effective secondary avalanche time t_i, from Putnam, is about 0.1 nsec.

Furthermore, we assume that ion avalanche decays exponentially with a characteristic time t_d after neutralization occurs. Crudely, we suppose that $t_d(P)$ scales inversely with pressure below the 36 mTorr ion avalanche cutoff, and that near cutoff it approaches 5 nsec. Then the ion avalanche contribution to the ionization rate would be reduced by a factor of $\exp\{-tP\,(\text{Torr})/[0.18\,(\text{nsec})]\}$. Also note that we must recalculate τ_n to include ion avalanche.

We then have

$$\frac{dn_e(t)}{dt} = \begin{cases} 0; & t<\tau_n, \\ \dfrac{n_b(t)}{0.4}P(\text{Torr}) + \dfrac{n_i(\tau_n)}{0.07}P(\text{Torr})\exp\left(\dfrac{(t-\tau_n)P(\text{Torr})}{0.18}\right) + \dfrac{n_e(t)}{0.1}; & \tau_n<t<t_b, \\ \dfrac{n_b(t)}{0.4}P(\text{Torr}) + \dfrac{n_i(\tau_n)}{0.07}P(\text{Torr})\exp\left(\dfrac{(t-\tau_n)P(\text{Torr})}{0.18}\right); & t_b<t<t_{\text{beam}}, \\ \dfrac{n_i(\tau_n)}{0.07}P(\text{Torr})\exp\left(\dfrac{-tP(\text{Torr})}{0.18}\right); & t>t_{\text{beam}}, \end{cases} \tag{6}$$

and

$$\frac{dn_i(t)}{dt} = \begin{cases} \dfrac{n_b(t)}{\tau_e} + \dfrac{n_i(t)}{t_{ia}} & t<\tau_n \\ \dfrac{dn_e(t)}{dt} & t>\tau_n. \end{cases} \tag{7}$$

These yield the $\omega_p\,(t, P)$ exhibited in Fig. 6.

The rapid avalanching leads to high ion and electron densities in less than 40 nsec, if $P>10$ mTorr. The plasma frequency rises rapidly through our observing window (10 GHz $<f\leqslant$ 40 GHz) for early times less than or equal to 20 nsec. However, there will always be regions of low beam current near the chamber edge where the beam does not ionize rapidly and ω_p is lower. These regions may produce emission at low frequencies.

The rapid rise of $\omega_p(t)$ above 10 mTorr explains why emission above 7 GHz is "spiky" in time. Each channel shows high power as $\omega_p(t)$ passes through that band, and little thereafter.

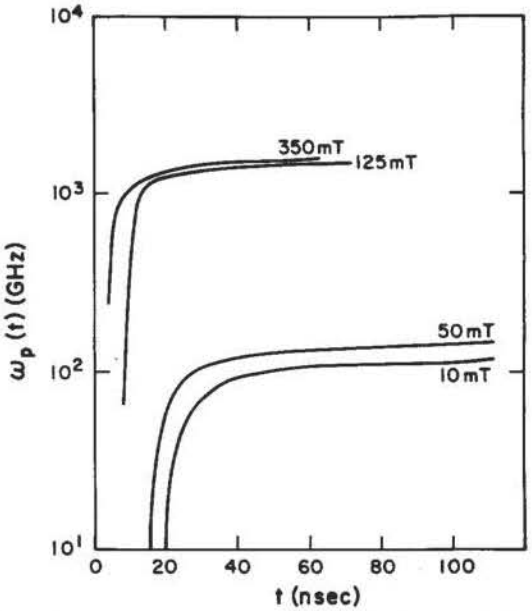

FIG. 6. Avalanche production of plasma, leading to rapid increases of plasma frequency in time.

IV. RADIATION MECHANISMS

The electron beam will break down air and cause avalanche ionization at about 0.01 Torr pressure. Below this pressure, direct ionization can partially compensate the beam charge, but we expect the dynamics will be ruled by the self-charge introduced into the chamber. There are two radiation mechanisms available: (a) oscillation of the "virtual cathode," a cloud of charge excess located probably several skin depths, c/ν_{pb} beyond the anode foil; (b) reflexing of electrons about the anode, i.e., oscillations driven by the attempt of electrons to flee the chamber by reversing themselves, only to find themselves stopped again as they approach the cathode.

We expect the movement of a charge cloud beyond the anode will be sensitive to boundary effects (close walls will bleed off the charge) and, because the whole cloud must move, to yield radiation in the region of a few harmonics of ν_{pb}, the beam plasma frequency is approximately 3 GHz. Reflexing, on the other hand, promises higher frequencies, since the field gradients are probably steeper nearer the cathode. Generally, both reflexing and virtual cathode emission can occur simultaneously. A qualitative signature of virtual cathode radiation should be persistent low-frequency power, while reflexing yields higher frequencies.

A single bunch of electrons radiating in phase, and correlated spatially over a distance L will produce a spectrum dependent on the spatial correlation function. A delta-function correlation $\delta(r\text{-}L)$ yields a flat spectrum. A Lorentzian bunch with width L emits an exponential spectrum for all wavelengths larger than L. A Gaussian form for the bunch yields a spectrum of approximately $\exp(-\nu^2)$, etc. The Lorentzian form clearly is compatible with the exponential spectra for 1 mTorr and 12 mTorr shown in Fig. 4, implying a bunch smaller than a centimeter. Figure 4 displays some low-frequency excess at 1 mTorr, though this is not clear evidence for a virtual cathode explanation. The strong flattening of the 12 mTorr spectrum versus the 1 mTorr argues for a reflexing mechanism dominating the emission, as plasma-producing collisions begin to neutralize the overall charge cloud in the chamber.

Once a dense plasma exists in the chamber, emission at $\omega_p(t)$, and its harmonics can easily account for the observed powers and spectrum, following theory developed for purely beam-plasma cases.[11–16] Reference 11 showed that small density fluctuations, $\delta n_b/n_b \approx 0.01$, can yield powers exceeding a megawatt. Emission above $2\omega_p$ can occur powerfully if $n_b/n_p > 0.01$, which may well occur briefly throughout the experiments above 10 mTorr. This further complicates the picture, making detailed calculation of the spectrum difficult.

All beam-plasma emission schemes require linear instability. The electron-neutral collision rate in the plasma can suppress plasma modes; however, if it exceeds the streaming growth rate,

$$\nu_{e-n} > (\pi/2)\,\omega_p\,(n_b/n_p)\gamma\theta^2, \tag{8}$$

where θ, the opening angle of the beam profile, is approximately 60° for our work.

We may, per Putnam,[9] set the electron density at $226\,n_b$ after gas breakdown; the gas density is then $10^{16}\,P$ (Torr) cm^{-3}. The collision cross-section is about 10^{16} cm^2 so $\nu_{e-n} \simeq 4\times 10^8\,P$ (Torr)/sec using an electron-air cross section for 10 eV electrons.

There will be a large range of n_b/n_p at the channel edges. When ω_p exceeds our uppermost observed frequency (40 GHz) we then observe emission from this edge region. This complicates the analysis, since n_b/n_b can vary greatly there. Equation (8) yields

$$P\,(\mathrm{Torr}) > 10\left(\frac{\nu}{10\ \mathrm{GHz}}\right)\left(\frac{T}{10\ \mathrm{eV}}\right)^{-1/2}\frac{n_b}{(n_p)}. \tag{9}$$

Thus n_b/n_p in the range 0.1 to 0.01 will yield the observed cutoff of ω_p emision at approximately Torr. This simple relation predicts that higher frequency emission requires higher pressures for cutoff, which is not observed, but the unknown pressure dependence of n_b/n_p near the channel edge obscures this point.

V. CONCLUSIONS

Collective processes yield microwave emission for $P \lesssim$ Torr, throughout our 10–40 GHz observing window. At pressures below approximately 10 mTorr, exponential spectra result, consistent with eigher beam reflexing or virtual cathode oscillations.

Above approximately 10 mTorr, the spectrum is flatter and power emitted falls linearly with pressures in all bands. Emission is spiky, probably because the plasma frequency passes through each band in about 20 nsec. Radiated power is consistent with earlier theory for beam-plasma instability, with emission at the local plasma frequency.

Emission falls below detectability (i.e., <1 kW) at approximately 3 Torr. This is consistent with suppression of beam-plasma streaming instability by electron–neutral collisions in the plasma.

By carefully preparing the beam in a 1 Torr chamber, we could propagate it about 1 m in air. Emission at about 10 GHz was weak but detectable.

ACKNOWLEDGMENTS

This work was supported by the Air Force Office of Scientific Research and the Office of Naval Research.

[1] P. H. deHaan, G. C. A. M. Janssen, H. J. Hopman, and E. H. A. Granneman, Phys. Fluids **25**, 592 (1982).
[2] Systems, Science, and Software APEX 107.
[3] S. G. Arutyunyan, O. V. Bogdankevich, Iu. F. Bondar, S. I. Zavarotni, A. Z. Ipatov, G. P. Mcheidze, A. A. Ovchinnikov, and A. A. Rukhadze, Plasma Phys. **25**, 11 (1983).
[4] G. Benford, J. Plasma Phys. **10**, 203 (1973).
[5] R. B. Fiorito, R. F. Fernsler, J. G. Greig, M. Herndon, I. M. Vitkovitsky, A. W. Ali, and V. E. Scherrer, Naval Reseach Laboratory Report No. 4405, 1973.
[6] E. J. Lauer, R. J. Briggs, T. J. Fessenden, R. E. Hester, and E. P. Lee, Phys. Fluids **21**, 1344 (1978).

[7]G. Wallis, K. Sauer, D. Sunder, S. E. Rosinskii, A. A. Rukhadze, and V. G. Rukhlin, Sov. Phys. Usp. **17**, 492 (1975).
[8]J. A. Nation and W. L. Gardner, Nucl. Fusion **11**, 5 (1971).
[9]S. Putnam (private communication).
[10]C. L. Olson, Phys. Rev. A **11**, 288 (1975).
[11]K. G. Kato, G. Benford, and D. Tzach, Phys. Fluids **26**, 3636 (1983).
[12]G. Benford and D. F. Smith, Phys. Fluids **25**, 1450 (1982).
[13]K. Papadopoulos and T. Coffey, J. Geophys. Res. **79**, 674 (1974).
[14]D. Whelan and R. L. Stenzel, Phys. Rev. Lett. **47**, 95 (1981).
[15]P. Y. Cheung, A. Y. Wong, C. B. Darrow, and S. J. Qian, Phys. Rev. Lett. **48**, 1348 (1982).
[16]M. V. Goldman, G. F. Reiter, and D. R. Nicholson, Phys. Fluids **23**, 388 (1980).